

Neutral hydrogen at high redshifts as a probe of structure formation – III. Radio maps from N-Body simulations.

J.S.Bagla[★], Biman Nath[†] and T.Padmanabhan[‡]

Inter-University Centre for Astronomy and Astrophysics, Post Bag 4, Ganeshkhind, Pune 411 007, INDIA

IUCAA Preprint 40/96

ABSTRACT

Large inhomogeneities in neutral hydrogen in the universe can be detected at redshifts $z \leq 10$ using the redshifted 21cm line emission. We use cosmological N-Body simulations for dark matter and a simple model for baryonic collapse to estimate the signal expected from structures like proto-clusters of galaxies at high redshifts. We study : (i) the standard CDM model, (ii) a modified CDM model with less power at small scales, and (iii) a Λ +CDM model in a universe with $\Omega_0 + \Omega_\Lambda = 1$. We show that it should be possible for the next generation radio telescopes to detect such structures at the redshift 3.34 with an integration of about 100 hours. We also discuss possible schemes for enhancing signal to noise ratio to detect proto-condensates at high redshifts.

Key words: Galaxies : formation – cosmology : theory – early Universe, large scale structure of the Universe

1 INTRODUCTION

It is generally believed that large scale structures like galaxies and clusters of galaxies formed from small initial inhomogeneities via gravitational collapse. One implication of this picture is a distinct epoch when structures like proto-galaxies and proto-clusters decoupled from the largely homogeneous universe. Present observations suggest that this epoch is around $z \sim 5$ for galaxies. Observations of structures in this stage of formation, if made, can be a very powerful constraint on the models of structure formation. Such observations will also improve our understanding of the process of structure formation.

Sunyaev and Zel'dovich (1972) [also see Sunyaev and Zel'dovich (1975)] pointed out that the formation of first structures may be probed by observing the redshifted 21cm line emitted by the neutral hydrogen in these structures. Several searches have been made to look for such structures at high redshifts. In absence of a detection, these searches have only been able to put limits on the mass of neutral hydrogen present in clumped form. For a summary of these surveys see Wieringa, de Bruyn and Katgert (1992) and references cited in that paper.

The Giant Meter-wave Radio Telescope (GMRT) presently being constructed in India should be able to im-

prove the observational situation considerably as regards the detection and study of proto condensates containing neutral hydrogen (Swarup 1984). The GMRT will be able to probe the redshifted 21cm line from three epochs centred at $z = 3.34$, 5.1 and 8.5. In this paper we will discuss the possibility of detection at the two lower redshifts.

Subramanian and Padmanabhan (1993) have computed the expected flux at these redshifts for some models of structure formation. They used the Press-Schechter formalism (Press and Schechter 1975) to compute the expected number densities of proto-clusters in the CDM and HDM models. In a later paper (Kumar, Padmanabhan and Subramanian 1995) they computed line profiles assuming the proto-clusters to be spherically symmetric. These studies suggest that it should be possible to detect proto-clusters in the standard CDM model using the GMRT with 10 to 20 hours of observations.

In this paper we will use N-Body simulations to follow gravitational collapse of dark matter and some simple approximations for estimating the collapsed and neutral fraction in dense regions to construct “radio maps” with same specifications as the GMRT. We will study these maps and suggest simple methods to optimise the signal to noise ratio.

Some authors have studied the distribution of neutral hydrogen at high redshifts using simulations that include gas dynamics, ionisation and other astrophysical processes. Most of these studies focus on small scale variations in the distribution of neutral hydrogen. [e.g. see (Weinberg et al. 1996)] However, the synthesised beam for the central square of the GMRT includes a large comoving volume in each pixel (approximately $8(h^{-1}\text{Mpc})^3$) and so the details of physical

[★] Present Address: Institute of Astronomy, Madingley Road, Cambridge CB3 0HA, U.K. e-mail : jasjeet@ast.cam.ac.uk

[†] E-mail: biman@iucaa.ernet.in

[‡] paddy@iucaa.ernet.in

processes operating at small scales can be ignored to a large extent. We can also ignore the differences in distribution of baryons and dark matter at small scales. Further, as we are interested in the neutral fraction at two epochs, we can choose to ignore the physical processes responsible for its evolution. This simplifies the problem to a large extent and we should be able to get meaningful estimates of the signal strength without a detailed treatment of baryons and astrophysical processes.

A brief discussion of the expected physical conditions at the epochs of interest is given below. These are the guiding considerations in choosing the simplifying assumptions for constructing the radio maps.

- $z = 3.34$: Observations show that the inter-galactic medium (IGM) is completely ionised (Giallongo E. et al. 1994) at this redshift. Numerical simulations suggest that nearly all of the neutral hydrogen is in high density, radiatively cooled objects (Weinberg et al. 1996). Observations show that a large fraction of mass in the damped Lyman- α absorption systems (DLAS), believed to be progenitors of present day galaxies, is in form of neutral hydrogen (Wolfe et al. 1995). Observations also show that the spin temperature of gas in DLAS, the relevant quantity for the 21cm transition, is much higher than the temperature of the background radiation at this epoch. It can be shown that, in such conditions, emission is the dominant mechanism and *the total energy emitted by radiators in such a state does not depend on the spin temperature* (Scott and Rees 1990).

- $z = 5.1$: We have very little information about the universe at this redshift. It is known that the intergalactic medium at redshifts $z < 5$ is fully ionised (Giallongo E. et al. 1994). It is believed that the process of ionisation is initiated by the first luminous structures in the universe. First structures like galaxies and quasars can form after $z \simeq 5-6$ in most models that satisfy other observational bounds. There are three possible scenarios that deserve mention.

- One possibility is that the universe was already reionised by $z = 5.1$. In this case the neutral hydrogen would be confined to dense regions like proto-galaxies and the intervening regions will be completely, or mostly, ionised.

- If the universe has been reheated by first luminous objects, but not reionised, then the spin temperature will be much higher than the temperature of the background radiation. A patchy reheating could lead to fluctuations in the 21cm emission at large scales (Madau, Meiksin and Rees 1997).

- If the universe is neither reheated nor reionised by $z = 5.1$ and the first luminous objects form around this epoch, then the spin temperature will be comparable to the temperature of the background radiation for models with $\Omega_b \leq 0.1$ (Scott and Rees 1990).

We will focus on the second scenario (for $z = 5.1$) and carry out all our calculations assuming that the universe is largely neutral and the spin temperature is much larger than the temperature of the radiation background. Fluctuations in spin temperature at large scales (Madau, Meiksin and Rees 1997) introduce uncertainty in the results as the region of interest may not have been reheated and hence the 21cm radiation will be much less than anticipated.

2 GENERATING RADIO MAPS

We will now outline the method that is used to construct radio maps by combining the distribution of dark matter obtained from N-Body simulations with approximations for the neutral fraction of gas. Radio observations with an interferometer give the flux of radiation coming from a given direction in the sky in a range of frequencies. This range of frequencies is subdivided into small equal intervals (channels). Within the field of view (primary beam) we can differentiate between flux from directions separated by an angle equal to the resolution of the interferometer (synthesised beam). Therefore we can arrange the information obtained from such an observation in terms of a radio map for each frequency channel. The angular resolution, or the pixel size, with which the map is constructed is given by the synthesised beam of the interferometer. For the purpose of generating “radio maps” from simulations, we will choose the parameters like pixel size and channel width to be same as that used by the GMRT central array (Swarup 1984). (The central array consists of 12 antennas of diameter 45m spread over a region of $1\text{km} \times 1\text{km}$. The telescopes are scattered randomly within this region.)

Earlier estimates of expected flux from high redshift objects have shown proto-clusters to be the most promising source (Subramanian and Padmanabhan 1993) of 21cm radiation. Observations of high redshift objects like quasars suggest that the intergalactic medium is completely ionised at redshifts $z < 4$. This implies that the only source of neutral hydrogen will be dense clouds inside galaxies. These clouds are sufficiently dense so that absorption in a thin layer near the surface shields the inner regions and a large fraction of the gas in these remains unionised. Therefore, while computing the flux, we must take into account the fact that the neutral hydrogen we observe resides in dense clumps and shares the internal velocity dispersion of these. We take this fact into account by convolving the line profile with a Gaussian of width 200km/s, at the epoch of emission. This consideration is relevant only for the window at $z = 3.34$ as in most models galaxies have not formed by $z = 5.1$. Any proto-galaxies that may exist are not expected to have any systematic velocity dispersion.

A remaining uncertainty in computing the amount of neutral hydrogen at high redshifts is the fraction of mass in galaxies at the epoch of interest. We will *reduce* the uncertainty due to this factor by considering only the regions with $\delta > 1$ in the numerical simulations. (Changing this threshold to $\delta > 3$ reduces the peak signal by less than 15%. Therefore the final result is not very sensitive to this threshold.) However, since this is a complex issue, we will only parameterise our ignorance with a factor f_{gal} which is the fraction of mass in galaxies that can hold neutral hydrogen. We will use $f_{gal} = 1$ but the results can be rescaled with any value. In a more detailed calculation, which can be done with N-Body simulations that use a much larger number of particles, individual halos of mass $M \geq 10^{10} M_\odot$ can be directly identified and the uncertainty parametrised by f_{gal} becomes irrelevant. This can not be done at present without reducing the physical size of the simulation box by a significant amount - in which case we will not be able to map all scales probed by the GMRT.

The radio map is generated from the N-Body data in the following manner:

- Use the co-ordinates of the particle to fix the pixel to which the contribution is to be added.
- Use the radial component peculiar velocity of the particle to compute the total redshift. Convolve the line profile with a Gaussian of width 200km/s and add the contribution to the relevant frequency channels.
- For generating maps at redshifts $z < 4$ impose a cutoff on density contrast $\delta \geq 1$ to ensure that we are looking at regions that can host galaxies.
- Repeat this process for all particles.

In the following subsections we will describe each of these components in greater detail. We begin by outlining the models of structure formation that are used for this study.

2.1 N-Body Simulations

We used N-Body simulations of three models to generate the “radio maps.” These were chosen from the family of CDM models and we used the parametrised spectrum given by Efstathiou, Bond and White (1992). These models were normalised using the root mean square amplitude of fluctuations in the temperature of the CMBR (Cosmic Microwave Background Radiation) observed by COBE (Wright et al. 1996).

All the simulations were carried out using 128^3 particles in a 128^3 mesh. The physical size of the box in each case was $128h^{-1}\text{Mpc}$. Thus the mass of each particle in these simulations equals $2.7 \times 10^{11} \Omega_0 M_\odot$.

The following parameters were chosen for these models :

- *Model I* : The standard CDM model (sCDM). ($\Gamma = \Omega_{nr}h = 0.5$, $\Omega_{nr} = \Omega_0 = 1$ and $h = 0.5$.) Normalisation with fluctuations in the CMBR gives $\sigma(8h^{-1}\text{Mpc}, z = 0) \simeq 1.2$ which is about twice the value implied by the abundance of rich clusters. This model is a reference model in studies of structure formation.

- *Model II* : A flatter version of the CDM model with $\Gamma = 0.3$, $\Omega_{nr} = \Omega_0 = 1$ and $h = 0.5$. The choice of Γ for this model is independent of the cosmological parameters. This model has $\sigma(8h^{-1}\text{Mpc}, z = 0) \simeq 0.6$ which is consistent with the observed amplitude of fluctuations at this scale. This model also predicts the correct slope of the correlation function at large scales. At large scales this model is a close approximation for some “flat” versions of CDM that can arise if a small but non-negligible fraction of mass in the universe is contributed by relativistic dark matter. (Mixed Dark Matter or MDM hereafter.)

- *Model III* : A Λ +CDM model (LCDM). ($\Gamma = \Omega_{nr}h = 0.3$, $\Omega_{nr} = 0.6$, $\Omega_\Lambda = 0.4$ and $h = 0.5$.) This model has $\sigma(8h^{-1}\text{Mpc}, z = 0) \simeq 1$ which is also consistent with the observed abundance of rich clusters. [The observed amplitude of fluctuations at the scale of $8h^{-1}\text{Mpc}$ scales approximately as $\Omega_{nr}^{-0.6}$ (White, Efstathiou and Frenk 1992).] This model satisfies most observational constraints that are available for cosmological models and models of structure formation. (Bagla, Padmanabhan and Narlikar 1996) (These constraints rule out large regions of the parameter space and only a small region survives. Therefore model III is a good

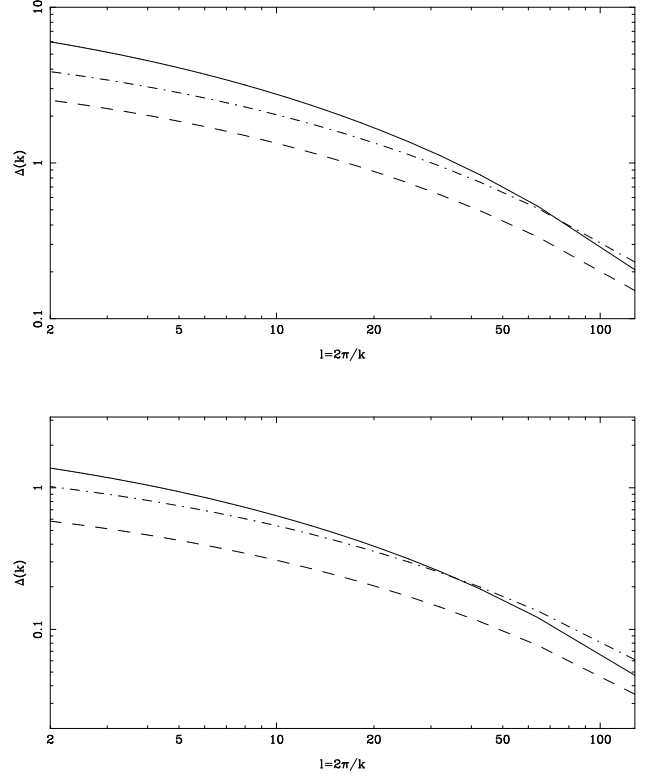


Figure 1. This figure shows the power spectra for the three models being discussed here. The standard CDM model is shown using a thick line, model II (MDM) as a dashed line and model III (LCDM) as a dot-dashed line in these panels. We have shown the linearly evolved power spectrum at the present epoch [top panel] and also at the redshift $z = 3.34$ [lower panel]. The different rate of growth for model III (LCDM) in the linear regime leads to an increase in the ratio of power in this model to the power in model I (sCDM) or model II (MDM).

example from the class of allowed models.) This model was chosen for two reasons :

- Growth of perturbations in a Λ model slows down at late epochs. In other words, such a model has more power at early times in comparison with an $\Omega_{nr} = 1$ universe which has same level of clustering at $z = 0$. Thus we have reason to expect higher signal for models in a universe with nonzero Λ .

- The comoving volume enclosed in a given solid angle at high redshifts is higher for a universe with nonzero Λ . This implies more emitters and hence a higher signal. In a model with nonzero cosmological constant the luminosity distance is also larger in comparison with the corresponding distance in the Einstein-de Sitter model for any given redshift. However, the increase in comoving volume mentioned above compensates for the increase in luminosity distance in such models.

We have shown the power spectra for these models in figure 1. To demonstrate the effect of different rate of growth in linear regime we have also shown the same spectra at redshift 3.34.

We would like to emphasise the following points regarding the choice of models: It is possible to choose many vari-

ants of the above models and repeat the analysis given in this paper. One can choose to normalise the power spectra in a different manner, e.g. by fixing the amplitude of perturbations at $8h^{-1}\text{Mpc}$ rather than at very large scales using COBE observations. Other parameters like the Hubble's constant, the cosmological constant, the density parameter and the primordial spectral index can also be varied from the values used here. We have consciously restricted ourselves to a small set of example models for the purpose of illustration. A more detailed exercise will be warranted if the GMRT succeeds in detecting neutral hydrogen at these redshifts and a more meaningful comparison with models can be carried out using real data.

2.2 Evolution of Neutral Fraction

Generating artificial radio maps requires, in principle, a detailed knowledge of the distribution of baryons and the neutral fraction etc. However, as mentioned earlier in this paper, the comoving volume enclosed in each pixel is very large and therefore we can get reasonable estimates by assuming the distribution of baryons and dark matter to be the same. In the following discussion we will demonstrate, using a simple model, that the assumption of a constant neutral fraction at these scales is not very far from the truth. We will also show that our choice of $f_N = 0.5$ for $z = 3.34$ is not unrepresentative. We will show that the neutral fraction of gas in galaxies is largely independent of the depth of the potential well. In the following discussion we estimate the neutral fraction by using the model of star formation in galaxies of Kauffmann, White and Guiderdoni (1993; hereafter KWG). Here we will briefly summarise the relevant features of their model and use these to estimate the evolution of neutral fraction.

In this model, dark matter halos are assumed to be truncated singular isothermal spheres and it is assumed that the temperature T of the gas is given in terms of the circular velocity, V_c , as, $T = 35.9 (V_c/\text{km/s})^2 \text{ K}$. The virial radius r_v is defined to be the radius within which the mean overdensity is 200 (i.e., $r_v = 0.1H_0^{-1}(1+z)^{-3/2}V_c$). The radius where the cooling time of the gas is equal to the age of the universe is defined as the cooling radius, r_{cool} .

Suppose that the fraction of the critical density that is in baryons is Ω_b and f_g is the fraction of the baryons in the form of gas. The amount of cold gas inside the halo at time t is given by the amount of gas with cooling time $t_{cool} < t$. When $r_{cool} \gg r_v$, cooling is very rapid and the rate of increase of cold gas in the halo is governed by the accretion rate of the halo, (White and Frenk 1991)

$$\dot{M}_{inf}(V_c, z) = 0.15 f_g \Omega_b V_c^3 G^{-1}. \quad (1)$$

In the other limit, $r_{cool} \ll r_v$, the rate of inflow of cold gas can be written as,

$$\dot{M}_{cool}(V_c, z) = 4\pi\rho_g(r_{cool})r_{cool}^2 \frac{dr_{cool}}{dt}, \quad (2)$$

where $\rho_g(r)$ is the gas density at radius r .

In the model of KWG, the rate at which cold gas settles inside the halo is given by $\min(\dot{M}_{inf}, \dot{M}_{cool})$. For the cooling of the gas, we use the cooling function of Fall and Rees (1985) for a primordial gas, since the metallicity is any way small for gas at high redshift.

However, with the onset of star formation, the supernovae will begin to heat the gas. Following KWG, we assume that the number of supernovae per solar mass of stars formed is $\eta_{SN} = 4 \times 10^{-3} M_\odot^{-1}$. If each of the supernovae have a kinetic energy of the ejecta of order 10^{51} erg , and a fraction ϵ of this energy is used to heat the cold gas, then the rate of loss of cold gas to the hot phase of the interstellar medium is, (Kauffmann, White and Guideroni 1993)

$$\dot{M}_{reheat} = \epsilon \frac{4}{5} \frac{\dot{M}_* \eta_{SN} E_{SN}}{V_c^2}. \quad (3)$$

Here, \dot{M}_* is the star formation rate, which is given in this model as,

$$\dot{M}_* = \alpha \frac{M_{cold}}{t_{dyn}}. \quad (4)$$

Here t_{dyn} is the dynamical time. The authors defined the dynamical time as (where $\lambda \sim 0.05$ is the initial dimensionless spin parameter of the gas),

$$t_{dyn} = \frac{r_{gal}}{V_{gal}} = \frac{(2\lambda r_{vir})^{3/2}}{(GM_{gal})^{1/2}}. \quad (5)$$

These equations govern the evolution of the amount of cold gas, or, in other words, the neutral fraction f_{HI} , of gas in a halo of circular velocity V_c at a given redshift z , for an assumed value of the onset of inflow of gas z_{in} , and given the values of α and ϵ . Gas is assumed to be fully ionised at z_{in} . KWG estimated the values of α and ϵ from evolving the stellar population according to the above model and comparing the mean luminosity and the cold gas content of halos of $V_c = 220 \text{ km/s}$ with the observed values for the Milky Way [their Table 1]. For example, for $\Omega_0 = 1$, $\Omega_b = 0.1$, $\alpha = 0.1$, and $\epsilon = 0.08$. The values of α and ϵ are smaller for smaller values of Ω_b . However, we have found that the neutral fraction is not very sensitive to the values of α and ϵ , but rather to z_{in} .

We plot in figure 2 the neutral fraction f_{HI} at $z = 3.34$ for $z_{in} = 4, 5, 6, 9$, as functions of the rotational velocity V_c . It is seen that the neutral fraction is not sensitive to the value of V_c , for $V_c > 150 \text{ km/s}$. We will, therefore, use a constant value of f_n for all potential wells. We also show the values of f_{HI} at $z = 5.1$ for $z_{in} = 6, 9$ as functions of V_c in figure 2. The neutral fraction f_n does not depend very strongly on the value of $f_g \Omega_b$. In the following discussion we will use $f_n = 0.5$.

2.3 Redshift Space Projection

Simulations output the data in form of positions and velocities of particles whereas radio observations detect the flux as a function of angular position and frequency. In this subsection we will outline the method used for computing the observed central frequency around which the 21cm radiation from hydrogen atoms represented by a given N-Body particle is observed.

The peculiar velocity of an N-Body particle is given by

$$\mathbf{v}_p = a\dot{a} \frac{d\mathbf{x}}{da} = H_0 a^2 \frac{H(a)}{H_0} \frac{d\mathbf{x}}{da} \quad (6)$$

We only need the radial component of velocity for computing the redshift. As we are dealing with particles at very high redshifts we can align one axis of the simulation box

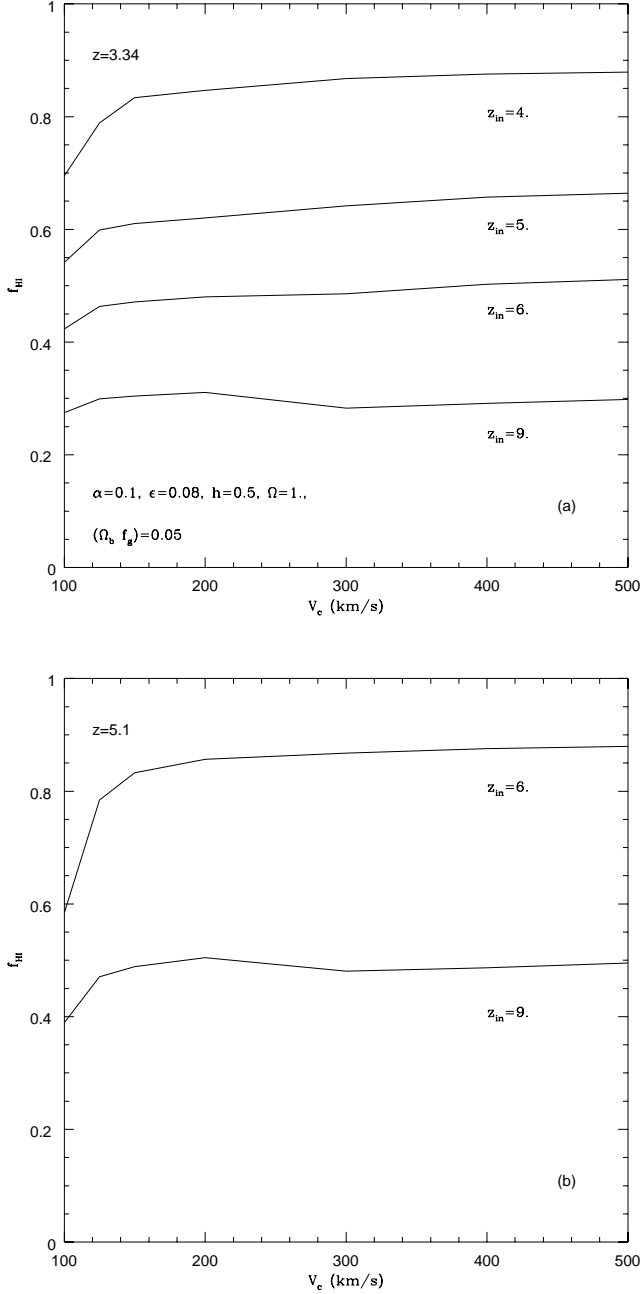


Figure 2. The upper panel shows neutral fraction f_{HI} at $z = 3.34$ against the circular velocity V_c of the halo for $z_{in} = 4, 5, 6, 9$. We have assumed $\alpha = 1$, $\epsilon = 0.08$, $f_g \Omega_b = 0.05$, $h = 0.5$ and $\Omega = 1$. Here, f_g is the fraction of baryonic mass in the form of gas. The curves do not strongly depend on the value of f_g . The lower panel similarly plots the neutral fraction at $z = 5.1$ for $z_{in} = 6, 9$.

along the line of sight and use that component of velocity for computing the recession velocity. The ratio of H/H_0 is given by

$$\frac{H(a)}{H_0} = \frac{\Omega_{nr}}{a^3} + \Omega_\Lambda \quad (7)$$

for the models of interest. The effective redshift results from

a combination of the Hubble recession and the peculiar velocity.

$$1 + z_{tot} = (1 + z_{hub})(1 + z_{pec}) \quad (8)$$

The average z_{hub} for the simulation box is $1/a - 1$. Redshift due to peculiar velocity is given by $z_{pec} = v_p/c$ where c is the speed of light.

2.4 Flux

If the spin temperature of the atoms emitting 21cm radiation is much greater than the temperature of the CMBR then the spin temperature drops out of the expression for the emitted energy. In such a case the energy dE emitted by a set of hydrogen atoms in an interval dt_e is given by

$$\begin{aligned} dE &= \text{Rate of Transition} \times \text{Energy carried by a photon} \\ &\quad \times \text{Number of hydrogen atoms} \times dt_e \\ &= \frac{3}{4} A_{21} \times h\nu_e \times \frac{M_{HI}}{m_p} dt_e \end{aligned} \quad (9)$$

where m_p is the mass of a proton and M_{HI} is the total mass in neutral hydrogen. We will use the mass in neutral hydrogen contributed by one particle in the N-Body simulation to compute total energy emitted by each “N-Body particle”. The mass M_{HI} is given by

$$\begin{aligned} M_{HI} &= M_{part} f_b f_n = M_{part} \frac{\Omega_b}{\Omega_0} f_n \\ &= 8.1 \times 10^9 M_\odot \left(\frac{\Omega_b}{0.06} \right) \left(\frac{f_n}{0.5} \right) \end{aligned} \quad (10)$$

here f_b is the fraction of baryons, Ω_b is the contribution of baryons to the density parameter and f_n is the neutral fraction. We have chosen $\Omega_b = 0.06$ as this value compares well with the observed abundance of light elements and primordial nucleosynthesis (Copi, Schramm and Turner 1995). Using this, we can estimate the flux received by an observer from an “N-Body particle”. For $\Omega_{nr} = \Omega_0 = 1$ models the flux contributed by one particle at redshift $z = 3.34$ is given by

$$S_\nu = 1.1 \mu Jy \left(\frac{M_{HI}}{8.1 \times 10^9 M_\odot} \right) \left(\frac{\Delta\nu_0}{175 kHz} \right)^{-1} \quad (11)$$

The frequency width used here corresponds to a velocity dispersion of 200km/s. (The corresponding number for the model with $\Omega_\Lambda = 0.4$ is $0.77 \mu Jy$.)

3 RESULTS

In this section we shall outline the results of analysis of the radio maps generated from N-Body simulations. We begin with a pictorial preview of the radio maps. Figure 3 shows a sample radio map for each of the three models at redshift $z = 3.34$. The panels of this figure show one frequency channel (chosen to be 125kHz; which - in velocity units - corresponds to about 115km/s.) The contours in these radio maps correspond to 15, 30 and $60 \mu Jy$. The pixel size is 3.2 arc minutes and it corresponds to a comoving scale of $2.7 h^{-1} \text{Mpc}$ for models I and II. ($3.5 h^{-1} \text{Mpc}$ for model III.) It is clear from these panels that models I (sCDM) and III (LCDM) have comparable signal whereas model II (MDM), as it has less power at smaller scales, has somewhat lower

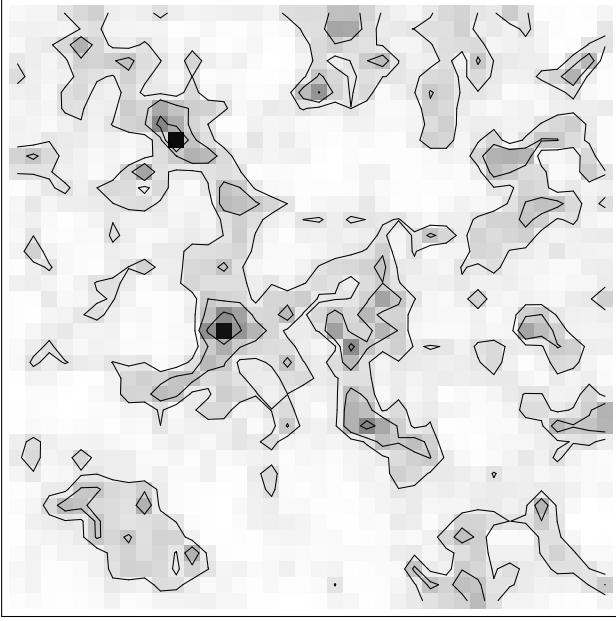


Figure 3. This figure shows a sample radio map for model I (sCDM) at redshift $z = 3.34$. This map is shown for one frequency channel of width 125kHz [corresponding to a velocity width of 115km/s]. Each pixel corresponds to an angular resolution of 3.2 arc minutes and a physical scale of about $3h^{-1}$ Mpc. The contour levels correspond to 15, 30 and $60\mu\text{Jy}$.

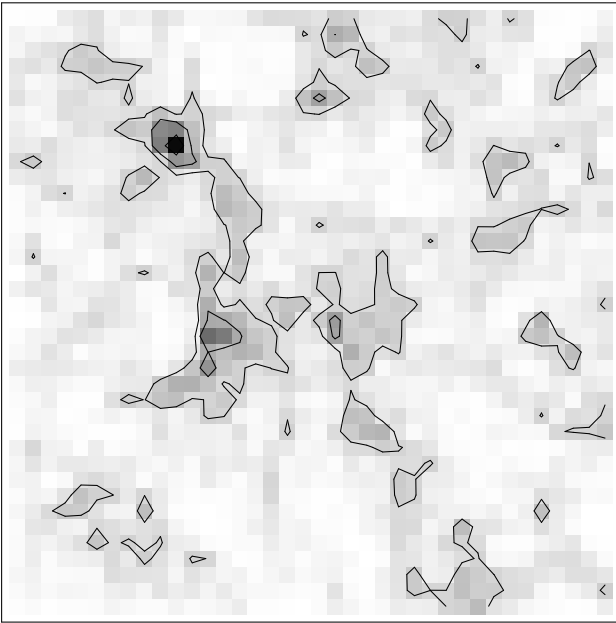


Figure 3. Continued. This figure shows a sample map for model II (MDM).

signal. The profile of peaks in the sCDM model is steeper than that in the LCDM model.

Figure 4 shows similar maps for $z = 5.1$ [$\nu_o = 233\text{MHz}$]. The width of one channel in this case corresponds to a velocity width of 161km/s. Angular size of each pixel is 4.5 arc minutes and this corresponds to a comoving scale of $4.7h^{-1}$ Mpc for models I (sCDM) and II(MDM). ($5.4h^{-1}$ Mpc

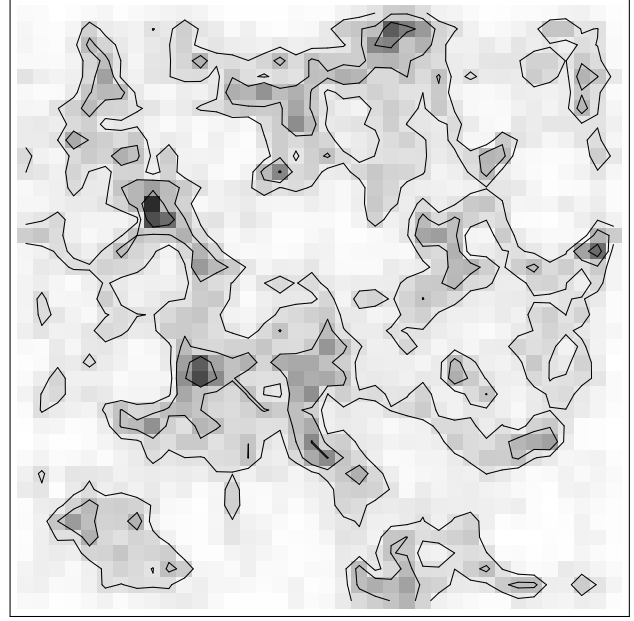


Figure 3. Continued. This figure shows a sample map for model III (LCDM).

for model III (LCDM).) These maps clearly show that there are no small scale structures in these, in comparison with the maps at $z = 3.34$. One reason for the gentler variation in signal from one pixel to another arises from the fact that, having assumed that the IGM is not ionised, we have not discarded matter in under dense regions while computing the signal. The signal is much higher as the comoving volume enclosed in each pixel/channel is larger than the corresponding volume at redshift 3.34.

These qualitative features can also be seen in figure 5 that shows a sample spectrum from the simulations of model III (LCDM) at these two redshifts. The spectra are shown as a function of channel number and the signal is shown in μJy . The typical width of high peaks seen in these graphs are much larger than the velocity dispersion of 200km/s ascribed to individual particles.

In order to make quantitative estimates of the possibility of detecting neutral hydrogen at high redshifts we computed the amplitude of three highest peaks in the radio maps for the three models. Table 1 lists the amplitudes and the full width at half maximum for these models for the three highest peaks in each case at redshift 3.34. The last column lists the number of pixels enclosed within the contours of half maximum. The contours were drawn for signal averaged over frequency channels. The number of channels used for averaging was taken to be the FWHM for the relevant peak. This number indicates the typical angular size of a flux peak and the signal can be smoothed at this scale to enhance signal to noise ratio. However, the shapes of these peaks are somewhat arbitrary and it is difficult to suggest a generic smoothing function for improving chances of detection. Figure 6 shows contours around one such peak, showing the level at which the signal drops to .75, .5 and .25 its maximum value. This figure demonstrates the point mentioned above regarding shapes of these contour.

Even though we cannot suggest the most optimum

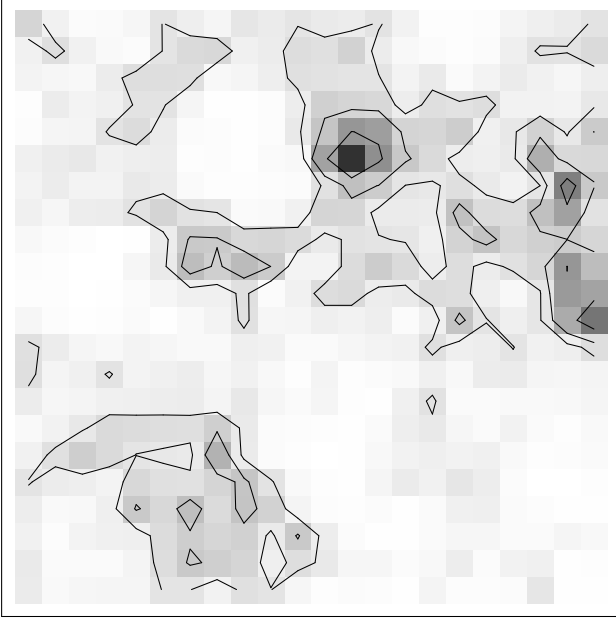


Figure 4. This figure shows a sample radio map for model I (sCDM) at redshift $z = 5.1$. This map is shown for one frequency channel of width 125kHz (corresponding to a velocity width of 160km/s). Each pixel corresponds to an angular resolution of 4.5 arc minutes and a physical scale of about $5h^{-1}$ Mpc. The contour levels correspond to 40, 80, 120 and $200\mu\text{Jy}$.

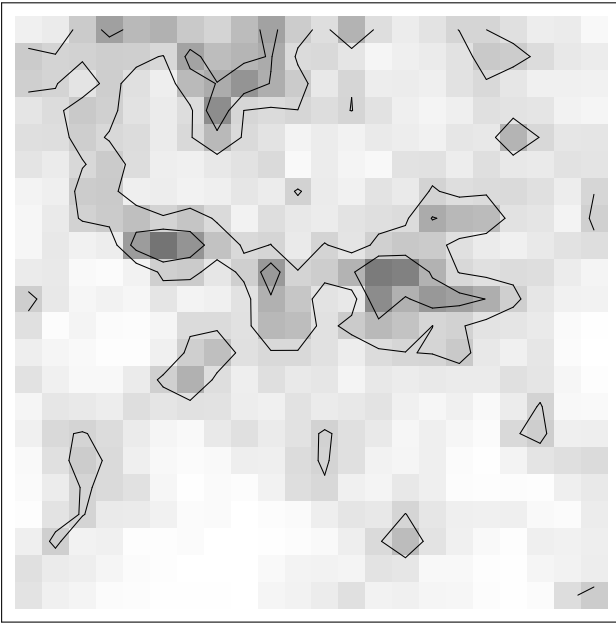


Figure 4. Continued. This figure shows a sample map for the MDM model (model II).

smoothing function for improving the signal to noise ratio, we have confirmed that the signal to noise ratio does improve for smoothing with a square top hat window of size $\approx n_{HM}^{1/2}$ where n_{HM} is the number of pixels enclosed within the contour of $S_{max}/2$. We assumed that the noise scales as $n^{-1/2}$ for small n . The signal to noise ratio for models II (MDM) and III (LCDM) can be improved by a factor

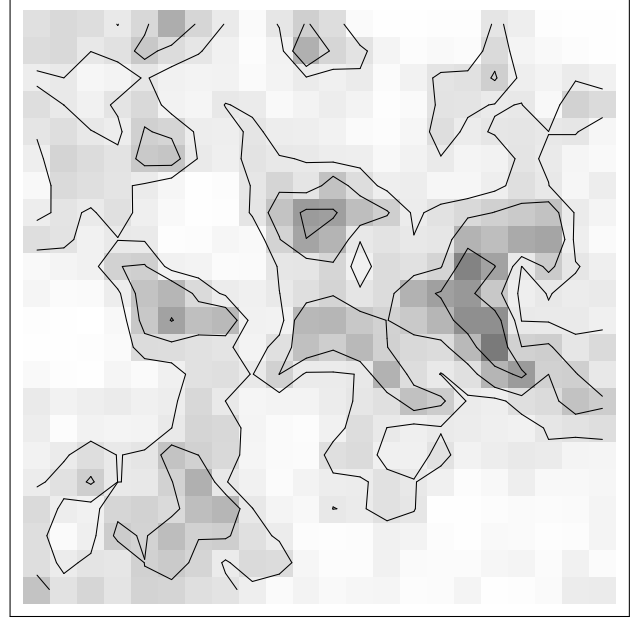


Figure 4. Continued. This figure shows a sample map for the LCDM model (model III).

Model	Amplitude (μJy)	FWHM (MHz)	n_{HM}
I	137.2	1.5	3
	101.5	1.0	11
	99.8	0.875	7
II	87.1	1.0	6
	97.7	0.75	8
	93.5	0.875	12
III	124.6	0.875	11
	111.3	0.875	13
	103.8	1.125	8

Table 1. This table lists details of three highest peaks in the simulated radio maps for the three models of structure formation being considered here for the redshift window at $z = 3.34$ (327MHz). We have listed the amplitude of peaks in micro Janskys, full width at half maximum in MHz and the number of pixels enclosed in the contours of half maximum. It is clear that models I (sCDM) and III (LCDM) have a higher signal as compared to model II (MDM).

two in this manner. The standard CDM model [model I] has more small scale power and hence the peaks are much sharper and therefore the gain in signal to noise ratio by smoothing is somewhat limited in this case.

In order to estimate the integration time required for detection and imaging of these peaks we need to know the root mean square amplitude of noise expected for the GMRT receivers. The expected noise for the central array is

$$\begin{aligned}
 \text{rms noise} &= 44\mu\text{Jy} \left(\frac{T_s}{110\text{K}} \right) \left(\frac{1\text{MHz}}{\Delta\nu} \right)^{1/2} \left(\frac{100\text{hrs}}{\tau} \right)^{1/2} \\
 &= 100\mu\text{Jy} \left(\frac{T_s}{250\text{K}} \right) \left(\frac{1\text{MHz}}{\Delta\nu} \right)^{1/2} \left(\frac{100\text{hrs}}{\tau} \right)^{1/2}
 \end{aligned}$$

The system temperature for 327MHz window is 110K and the corresponding number for 233MHz is 250K. (Swarup 1984)

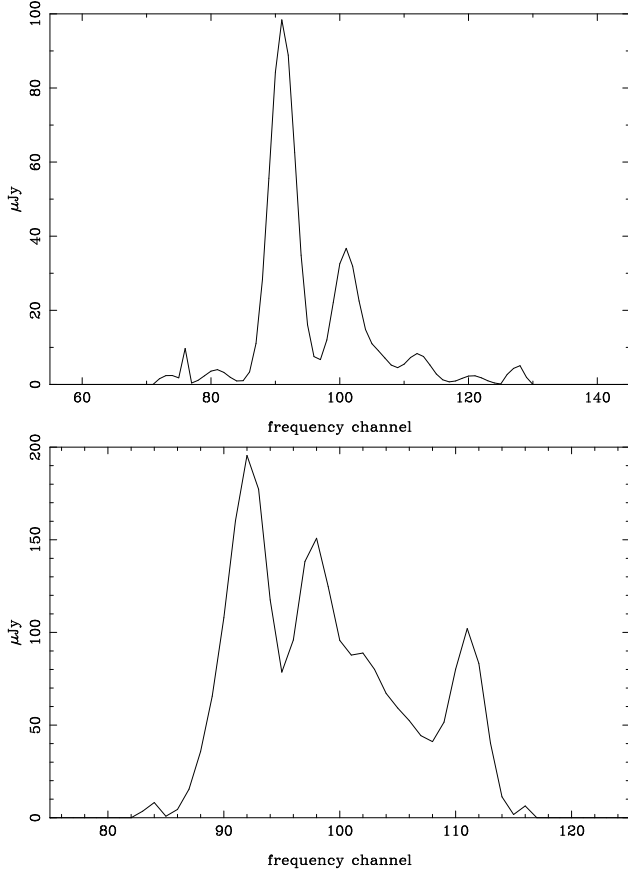


Figure 5. This figure shows a sample spectrum for each of the redshifts. The spectra shown here are taken from the simulated radio maps of the LCDM model (model III). The top panel corresponds to $z = 3.34$ and the lower panel to $z = 5.1$. The signal in μJy is shown as a function of frequency channel [channel width=125KHz]. This figure shows that the signal at $z = 5.1$ has few small scale variations in comparison with the signal at $z = 3.34$.

It is clear from table 1 that the peak signal expected in models I (sCDM) and III (LCDM) is about three times larger than the rms noise expected at redshift 3.34. Further, the width of the peaks in frequency space is comparable to 1MHz. The signal to noise level can be enhanced further by smoothing over nearby pixels. The number of pixels enclosed in the contour of $S_{max}/2$ for model III (LCDM) varies between 8 and 13 for the three higher peaks listed in table 1. Therefore an enhancement by a factor two or more can be obtained by smoothing over nearby pixels. This implies that a 3σ detection of such objects should be possible with an integration time of 50 – 100hrs. The main uncertainty in this result comes from our lack of knowledge about the fraction of mass in galaxies. We have, of course, tried to reduce the uncertainty by using only regions with density contrast greater than unity for computing the signal. As mentioned before, we find that changing the density threshold to $\delta_c = 3$ does not change the amplitude of the highest peaks by more than 15%. However, as the estimated signal and noise have a similar amplitude, even a small factor may make all the difference.

Detection of neutral hydrogen at high redshift for model I (sCDM) should also require similar integration time.

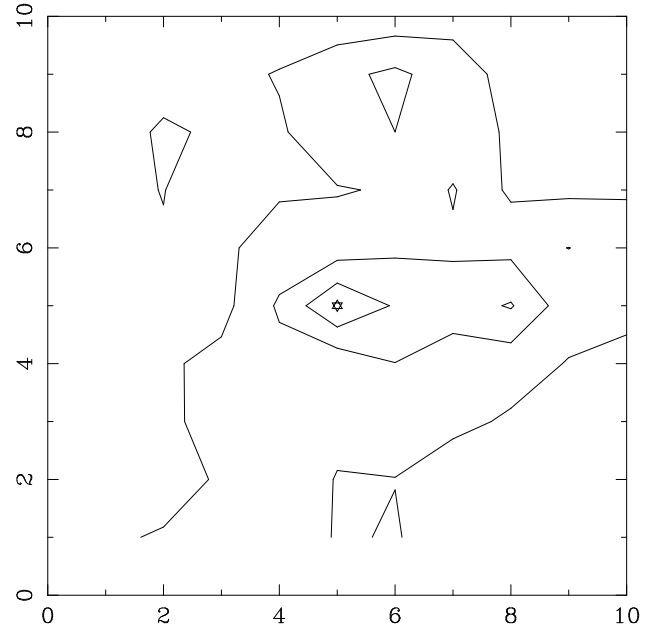


Figure 6. This figure shows the contours for $f * S_{max}$ around a peak for $f = 0.75, .5$ and 0.25 . These contours are for one of the highest peaks in simulated maps for model III (LCDM). The peak is located at (5,5) in this picture and is marked by a star. It is clear from this figure that the signal can be averaged over neighbouring pixels to improve signal to noise ratio. However the shape of this contour suggests that the amount of gain from such an optimisation will be limited.

Here the frequency spread of the highest peak is very large and compensates, to some extent, the compactness of the peak in angular co-ordinates. On the other hand detection of neutral hydrogen in model II (MDM) is a more difficult proposition as the peak signal is small compared to that for the other two models. The integration time required for model II (MDM) is at least twice as large as that for models I (sCDM) and III (LCDM).

Table 2 lists the amplitude of three highest peaks for the three models we are using here for the window at redshift 5.1. We have also listed the full width at half maximum for each of these peaks. These peaks have a very shallow profile and the number of pixels, enclosed within the region where the signal is greater than half of the maximum value, can be very large. Therefore we can smooth the signal over a few neighbouring pixels and improve the signal to noise ratio by a significant amount. Results for different models in this case are:

- Model III (LCDM) predicts a signal that is comparable to the rms noise. Smoothing over nearby pixels and integration for 50 – 100hrs should be sufficient for a 3σ detection.
- Model I (sCDM) also predicts signal at the same level as model III (LCDM).
- Model II (MDM) has very low signal as compared to models I (sCDM) and III (LCDM) and will require an integration for 100 – 200 hours for a 3σ detection.

These numbers, however, must be considered in light of the possibility of a patchiness in reheating of the IGM. (Madau, Meiksin and Rees 1997)

Model	Amplitude (μJy)	FWHM (MHz)
I	199.0	0.75
	181.4	1.0
	163.2	0.625
II	138.6	0.75
	115.2	0.875
	103.8	0.75
III	221.7	0.75
	195.6	0.875
	153.9	0.875

Table 2. This table lists details of three highest peaks in the simulated radio maps for the three models of structure formation being considered here for the redshift window at $z = 5.1$ (233MHz). We have listed the amplitude of peaks in micro Janskys and full width at half maximum in MHz. It is clear that models I (sCDM) and III (LCDM) have a higher signal as compared to model II (MDM).

4 DISCUSSION

Results of numerical simulations suggest that it could be possible to detect neutral hydrogen at high redshifts, in proto-clusters. Detection of these objects with the GMRT will require integration over 50 – 100 hours. The signal to noise ratio for $z = 3.34$ is better than that expected for $z = 5.1$ if we choose the factor f_{gal} to be unity. This is the most uncertain number in our calculation. If this number is much smaller than unity then it may be difficult to image proto-clusters at this redshift. It may still be possible to “detect” neutral hydrogen statistically by doing a $(\Delta T)/T$ type of an experiment. In these one looks for excess correlations than are expected from noise in the instrument. For example, the emission from a region of size $10^6 (h^{-1}\text{Mpc})^3$ - typical size of the volume probed in one field of view - is around $370mJy$. [This number is obtained by using the average flux in the simulated radio maps.] This will appear as excess noise if the individual structures can not be imaged. Integration over more than one field of view can also be used to enhance the chances of detection as one may be able to pick up a rare density peak (Subramanian and Padmanabhan 1993).

As mentioned above, the biggest uncertainty in our results for $z = 3.34$ is introduced by our lack of knowledge about f_{gal} . This uncertainty can only be removed with large simulations that can resolve masses less than $10^{10}M_{\odot}$ and still cover a volume that is comparable with that covered by one field of view for the GMRT. The other option is to carry out a series of N-Body experiments at different scales for each of the models and deduce f_{gal} for each model from the ensemble of simulations.

A comparison with earlier estimates for the expected signal (Kumar, Padmanabhan and Subramanian 1995) shows that the highest signal obtained in simulations is smaller than that expected from a proto-cluster of mass $10^{15}M_{\odot}$. This could result due to three reasons

- We do not have a sufficiently high peak in our realisation of the density field.
- The angular extent of the proto-clusters is considerably larger than one pixel.

- The velocity dispersion of these clusters is larger than expected.

We feel that all of these factors have contributed to make our estimates smaller than the earlier estimates by a factor 2 – 5.

The possibility of detection of neutral hydrogen at redshift 5.1 may be easier if the universe has been reheated but not fully reionised. Another good feature of 21cm emission from this epoch is that it only has smooth large scale variations in signal and hence it should be possible to enhance the signal to noise ratio by at least a factor 2 – 3 by smoothing over nearby pixels. However, the results for this epoch are somewhat uncertain due to our poor knowledge of the physical conditions at $z > 5$.

ACKNOWLEDGEMENT

Authors thank K.Subramanian and J.Chengalur for useful discussions. JSB thanks CSIR India for financial support.

REFERENCES

- Bagla J.S., Padmanabhan T. and Narlikar J.V., 1996, *Comments on Astrophysics*, 18, 275
- Copi C.J., Schramm D.N. and Turner M.S., 1995, *Science*, 267, 192
- Fall S.M. and Rees M.J., 1985, *ApJ*, 298, 18
- Giallongo E. et al., 1994, *ApJ*, 425, L1
- Kauffman G., White S.D.M. and Guideroni B., 1993, *MNRAS*, 264, 201
- Kumar A., Padmanabhan T. and Subramanian K., 1995, *MNRAS*, 272, 544
- Madau P., Meiksin A. and Rees M.J., 1997, *ApJ*, 475, 429
- Press W.H. & Schechter P., 1975, *ApJ*, 187, 452
- Scott D. and Rees M.J., 1990, *MNRAS*, 247, 510
- Subramanian K. and Padmanabhan T., 1993, *MNRAS*, 265, 101
- Sunyaev R.A. and Zeldovich Ya.B., 1972, *A&A*, 20, 189
- Sunyaev R.A. and Zeldovich Ya.B., 1975, *MNRAS*, 171, 375
- Swarup G., 1984, *Giant Meter-Wavelength Radio Telescope - Proposal*, Radio Astronomy Centre, TIFR, India.
- van de Hulst, H.C., 1945, *Nederlandsch Tid voor Naturkunde*, 11, 201
- Weinberg D.H., Hernquist L., Katz N.S. and Miralda-Escudé J., 1996, *Cold Gas at High Redshift* eds. M. Bremer, H. Rottgering, G. Carilli and P. van de Werf, Kluwer, Dordrecht.
- White S.D.M., Efstathiou G. and Frenk C.S., 1992, *MNRAS*, 262, 1023
- White S.D.M. and Frenk C.S., 1991, *ApJ*, 379, 52
- Wieringa M.H., de Bruyn A.G. and Katgert P., 1992, *A&A*, 256, 331
- Wolfe A.M., Lanzetta K.M., Foltz C.B. and Chaffee F.H., 1995, *ApJ*, 454, 698
- Wright E.L., Bennet C.L., Gorski K., Hinshaw G. and Smoot G.F., 1996, *ApJ*, 464, L21